

# SCIENTIFIC REPORTS

OPEN

## Berberine alleviates hyperglycemia by targeting hepatic glucokinase in diabetic *db/db* mice

Meng Li<sup>1</sup>, Yanqi Dang<sup>1</sup>, Qiong Li<sup>1</sup>, Wenjun Zhou<sup>1</sup>, Jianping Zuo<sup>2</sup>, Zemin Yao<sup>3</sup>, Li Zhang<sup>1</sup> & Guang Ji<sup>1</sup>

Berberine (BBR) is a widely used anti-diabetic agent, and liver glucokinase (GK) has been reported to be involved. However, the mechanisms of BBR in regulating GK are still unknown. Here, we found that BBR upregulated GK immunofluorescence expression in AML12 cells cultured in high glucose and increased glycogen content simultaneously. BBR improved hyperglycemia in *db/db* mice, and increased liver glucose-6-phosphate/glucose-1-phosphate (G-6-P/G-1-P) was found by analyzing metabolites (serum, liver, and feces) based on gas chromatography-mass spectrometry (GC-MS) metabolomics. Pharmacokinetics-pharmacodynamics (PK-PD) assessment revealed enriched BBR distribution in the liver, and liver G-6-P had the same trend as the concentration-time curve of BBR. G-6-P is solely catalyzed by GK, and GK activity and expression showed a positive correlation with liver BBR levels. In *db/db* mice, BBR also upregulated GK in liver fractions (cytoplasm and nucleus) and liver glycogen content. GK functionally worked by dissociating from GK regulatory protein (GKRP), and although GKRP expression was not affected, we found a decreased ratio of GK binding with GKRP in BBR treated *db/db* mice. In conclusion, our study suggests the dissociation of GK from GKRP as the potential mechanism for liver GK increase upon BBR treatment, which contributes to the anti-diabetic effect of BBR.

The emergence of type 2 diabetes mellitus (T2DM) as a global pandemic is one of the major challenges to human health in the 21st century<sup>1</sup>. In 2015, 415 million people suffered from diabetes worldwide (IDE, 2015)<sup>2</sup>, and diabetes is estimated to be a heavy burden on health care in future decades.

The liver plays a crucial role in controlling glucose homeostasis by coordinating the metabolism, synthesis, storage, and redistribution of nutrients<sup>3,4</sup>. In postprandial status, the liver contributes to the disposal of enteral glucose loads by enhancing glycogen synthesis and suppressing hepatic glucose export<sup>5</sup>. In the fasting state, the liver produces glucose by glycogenolysis to maintain euglycemia. These physiological processes are dysregulated in T2DM, and this imbalance contributes to hyperglycemia in both postprandial and fasting states<sup>6</sup>. Hepatic glycogen thus delicately coordinates the release of glucose from the liver and regulates the homeostasis of glucose metabolism.

The transport of glucose into hepatocytes occurs through glucose transporter type 2 (GLUT2). Glucose can freely exit hepatocytes without transformation, and once it enters the cell, glucose will transform into glucose-6-phosphate (G-6-P) to limit its outflow. The transformation of glucose to G-6-P in hepatocytes is catalyzed solely by glucokinase (GK), which works as the gatekeeper for glucose metabolism in hepatocytes. G-6-P can be either further transformed to glucose-1-phosphate (G-1-P) and synthesized into glycogen for storage or utilized by the cell via the tricarboxylic acid cycle and pentose phosphate pathway. The activator of GK is reported to increase liver glucose uptake in male Sprague-Dawley and Zucker diabetic fatty rats<sup>7</sup>, indicating that GK could be a promising target for hyperglycemia. GK activity is largely regulated by its subcellular localization. Physiologically, GK regulatory protein (GKRP) binds to GK in the nucleus when concentrations of glucose are low, and dissociation occurs under high-glucose conditions; however, this coordination is damaged in diabetic status<sup>8,9</sup>.

<sup>1</sup>Institute of Digestive Diseases, China-Canada Center of Research for Digestive Diseases (ccCRDD), Longhua Hospital, Shanghai University of Traditional Chinese Medicine, 200032, Shanghai, China. <sup>2</sup>Laboratory of Immunology and Virology, Shanghai University of Traditional Chinese Medicine, 201203, Shanghai, China. <sup>3</sup>Department of Biochemistry, Microbiology & Immunology, Ottawa Institute of Systems Biology, University of Ottawa, K1H 8M5, Ottawa, Canada. Correspondence and requests for materials should be addressed to L.Z. (email: [zhangli.hl@163.com](mailto:zhangli.hl@163.com)) or G.J. (email: [jjliver@vip.sina.com](mailto:jjliver@vip.sina.com))

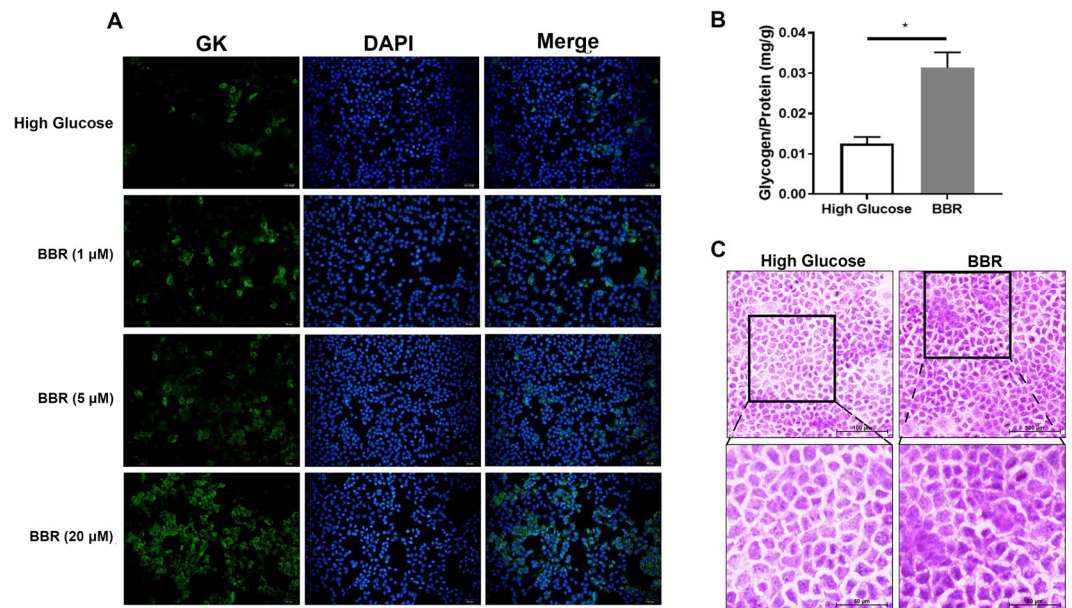


**Figure 1.** BBR promoted GK expression in AML12 cells. AML12 cells were maintained in high-glucose medium (17.5 mM) for 24 h in the presence or absence of BBR (1  $\mu$ M, 5  $\mu$ M, or 20  $\mu$ M). Immunofluorescence of GK expression in cells was visualized (A). AML12 cells were treated with 20  $\mu$ M BBR for 24 h, and glycogen content was chemically evaluated (B) and stained with PAS (C). Data are presented as the mean  $\pm$  SEM, and the experiments were performed in triplicate. \* $P < 0.05$  between groups.

Control of T2DM is urgent, and available agents include insulin sensitizers<sup>10</sup>, insulinotropic peptides<sup>11</sup>, and glucose absorption inhibitors<sup>12</sup>, among others. However, these strategies have limitations, and the long-term effect is far from ideal, making new agents greatly needed. In recent years, the interest in natural products that treat T2DM has grown. Berberine (BBR, C<sub>20</sub>H<sub>18</sub>NO<sub>4</sub>), a pharmacological component principally isolated from *Rhizoma coptidis* Franch. (family *Ranunculaceae*), which has long been widely used in traditional Chinese medicine for treating infectious diarrhea, has now been identified as a potential treatment for T2DM. Both clinical investigations and animal studies have confirmed its role in lowering blood glucose and improving related metabolic disorders<sup>13,14</sup>.

While the effect of BBR on T2DM has been confirmed, numerous studies have reported the possible mechanisms of BBR according to respective design and experiment data, making the mechanisms underlying the efficacy of BBR debatable. In alloxan-induced diabetic mice, it was reported that BBR increased GK expression and activity<sup>15</sup>, indicating GK as the possible target of BBR. However, this finding has not been verified by other studies, and the regulation mechanisms are unknown. In the present study, we used AML12 cells and diabetic *db/db* mice to investigate GK expression upon BBR treatment, applied metabolomics, pharmacokinetics-pharmacodynamics (PK-PD) assessment and molecular biological techniques to explore the regulatory mechanisms of BBR on GK. Our data might provide a systematic understanding of GK regulation under the anti-diabetic effect of BBR.

## Results

**BBR increased GK expression and glycogen content in AML12 cells.** To investigate the role of BBR in GK expression, we cultured AML12 cells in high-glucose medium, treated the cells with BBR (1  $\mu$ M, 5  $\mu$ M, or 20  $\mu$ M) for 24 h, and observed the GK fluorescence intensity. This revealed that 20  $\mu$ M BBR significantly increased GK expression, while the effect of low concentration (1  $\mu$ M and 5  $\mu$ M) BBR on GK was negligible (Fig. 1A). GK is the catalyzing enzyme of glucose metabolism in hepatocytes and contributes to glycogen synthesis. We also detected glycogen content, and glycogen content was significantly increased with 20  $\mu$ M BBR treatment (Fig. 1B). Periodic acid Schiff (PAS) staining of the cells further confirmed increased glycogen distribution under microscope observation (Fig. 1C).

**BBR alleviated hyperglycemia in *db/db* mice.** To evaluate the effect of BBR on diabetic *db/db* mice, we administered BBR to *db/db* mice for four weeks. The untreated *db/db* mice exhibited a diabetic phenotype, with average fasting blood glucose, hemoglobin A1c (HbA1c) and glucagon levels showing 2.7-fold, 1.5-fold, and 0.84-fold increases in comparison with the wild-type control mice ( $P < 0.001$ ). In contrast, BBR treatment significantly reduced these parameters, suggesting the anti-diabetic property of BBR ( $P < 0.001$ , Fig. 2A–C). Unexpectedly, we observed a remarkable decrease in serum insulin levels in *db/db* mice, and BBR significantly restored this decrease (Fig. 2D).

Liver glycogen serves as a form of energy storage and plays a pivotal role in regulating blood glucose. According to the PAS staining, glycogen deposition in the liver of *db/db* mice was significantly reduced, and

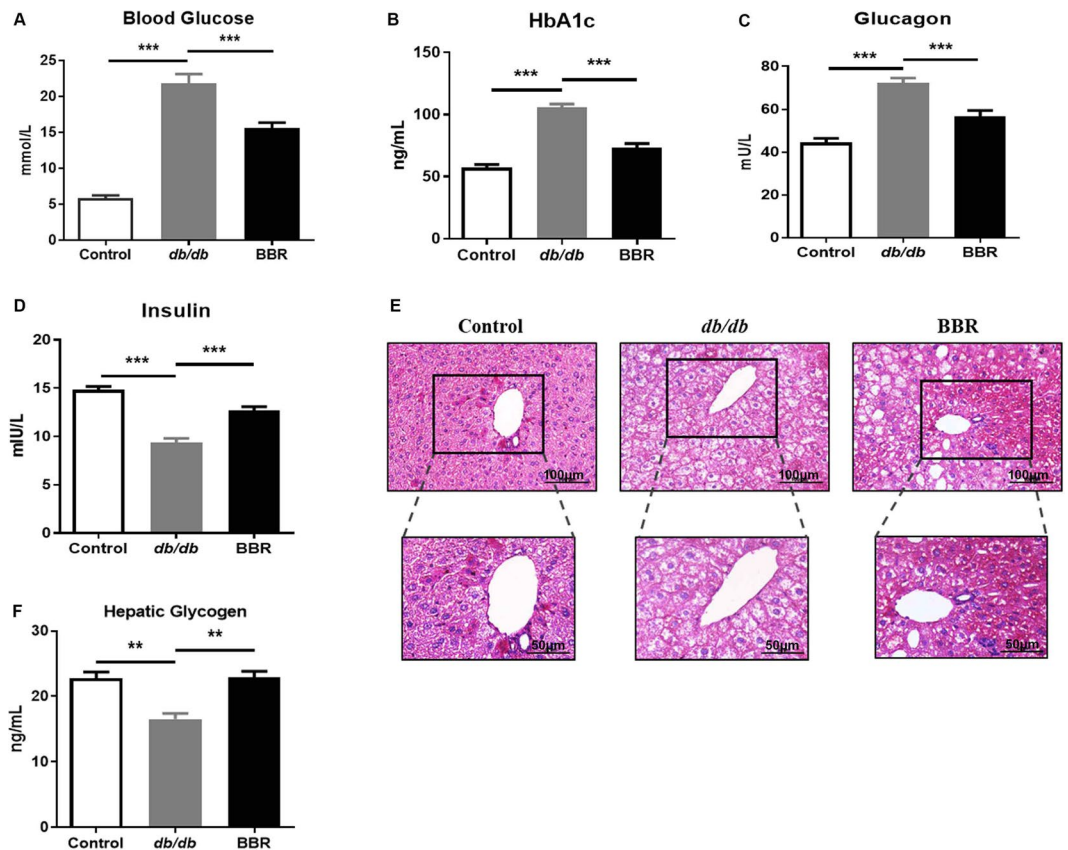


**Figure 2.** BBR alleviated hyperglycemia in *db/db* mice. Eight-week-old male *db/db* mice were treated with BBR ( $210 \text{ mg} \cdot \text{kg}^{-1} \cdot \text{day}^{-1}$ ) for 4 weeks, with untreated *db/db* mice and wild-type C57BL/6J mice used as controls. Blood glucose (A), HbA1c (B), glucagon (C) and insulin (D) levels were determined. Liver glycogen content (E) and representative PAS staining images (F, magnification was 200x and magnification of representative areas was 400x) were shown. Data are presented as the mean  $\pm$  SEM,  $n = 8$  per group.  $**P < 0.01$  and  $***P < 0.001$  between groups.

4-week BBR treatment significantly increased liver glycogen content (Fig. 2E). Biochemical analysis also confirmed the effect of BBR on liver glycogen increase (Fig. 2F).

**BBR altered the glucose-related metabolites in *db/db* mice.** To explore the possible mechanisms underlying the efficacy of BBR, we conducted metabolomics in serum, feces and liver samples of the mice. Differential metabolites were found between *db/db* mice and wild-type mice; glucose-related metabolites in serum (e.g., galactonic acid, arabinol, ribitol, xylitol, maltose, glycerol and sedoheptulose), feces (lactic acid, glucose, ribose, fructose, rhamnose, arabinose and lyxose) and the liver (fructose-6-phosphate, dihydroxyacetone phosphate, glycerate-3-phosphate, glucose, ribose-5-phosphate, gluconic acid, arabinol, galactonic acid, fructose, sedoheptulose and galacturonic acid) were significantly increased in *db/db* mice (Supplementary Table S1).

We next compared the glucose-related metabolites between BBR-treated and untreated mice, and a score plot of principal component analysis (PCA) completely separated the metabolites (serum  $R^2X = 0.717$ ,  $Q^2 = 0.283$ , feces  $R^2X = 0.524$ ,  $Q^2 = 0.166$  and liver  $R^2X = 0.527$ ,  $Q^2 = 0.0945$ ) of the two groups (Fig. 3A–C). Distinctly separated clusters were also shown by the partial least squares-discriminant analysis (PLS-DA) model (Fig. 3D–F). The evaluation parameters  $R^2X$ ,  $R^2Y$  and  $Q^2$  were 0.434, 0.923 and 0.687 in serum; 0.489, 0.995 and 0.933 in feces; and 0.378, 0.962 and 0.819 in liver samples, respectively. BBR-treated mice had different metabolic profiles from untreated mice. 12 metabolites (sucrose, maltose, ribitol, arabinol, glycerol-3-phosphate, xylitol, glycerol-2-phosphate, ribose, galactonic acid, pyruvic acid, glyceric acid, and glycerol) in serum, 6 in feces (glucose, gluconic acid, ribose, arabinol, glyceric acid and pyruvic acid) and 7 in liver samples (glucose, G-6-P/G-1-P, fructose-6-phosphate, gluconic acid, ribose-5-phosphate, dihydroxyacetone phosphate, and glycerate-3-phosphate) were significantly different between BBR-treated and untreated groups (Fig. 3G). BBR treatment decreased most of the glucose-related metabolites, which was consistent with the hypoglycemic effect (Table 1). However, hepatic G-6-P/G-1-P were found to be increased upon BBR intervention.

**PK-PD assessment.** An *In vivo* pharmacokinetic study in *db/db* mice treated with BBR was performed. The mean serum and liver concentration-time curves are shown in Fig. 4A,B. The maximum concentration ( $C_{max}$ ) of serum BBR was  $13.66 \text{ ng} \cdot \text{mL}^{-1}$ , the time to reach  $C_{max}$  ( $T_{max}$ ) was 2 h and the area under the concentration-time

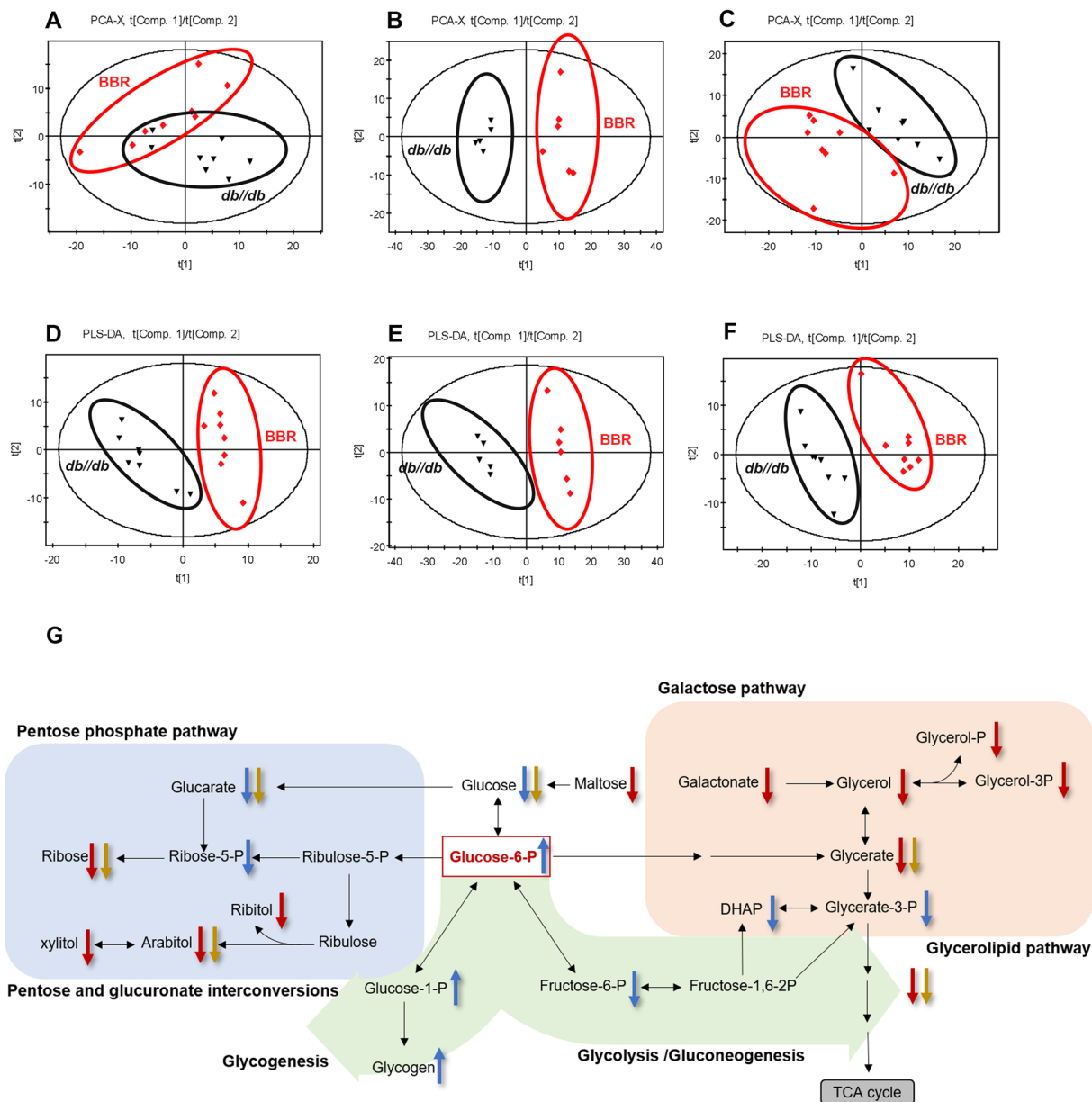


**Figure 3.** Metabolomics analysis of serum, liver and fecal samples. Metabolomics analysis was performed by GC-MS; PCA score plot of serum (A), liver (B) and feces (C), and PLS-DA score plot of serum (D), liver (E) and feces (F) from BBR-treated and untreated *db/db* mice are shown. (G) Glucose-related metabolites are summarized. Arrows pointing up and down represent increased and decreased metabolites, respectively, upon BBR treatment. Red arrows indicate changes in serum, blue indicates liver, and yellow indicates feces. Data are presented as the mean  $\pm$  SEM,  $n = 8$  per group. DHAP, dihydroxyacetone phosphate; Glucose-6-P, Glucose-6-phosphate; Glycerate-3-P, Glycerate-3-phosphate; Glycerol-2-P, Glycerol-2-phosphate; Glycerol-3-P, Glycerol-3-phosphate; Fructose-6-P, Fructose-6-phosphate; Fructose-1,6-2P, Fructose-1,6-diphosphate; Ribose-5-P, Ribose-5-phosphate; Ribulose-5-P, Ribulose-5-phosphate.

curve ( $AUC_{0-t}$ ) was  $87.26 \text{ ng}\cdot\text{h}\cdot\text{mL}^{-1}$  (Supplementary Table S3). In contrast, liver  $C_{max}$  was  $44.73 \mu\text{g/g}$ ,  $T_{max}$  was 2 h and  $AUC_{0-t}$  was  $173.00 \mu\text{g}\cdot\text{h}\cdot\text{g}^{-1}$  (Supplementary Table S4), indicating that orally administered BBR rapidly reached the liver and had higher concentrations.

We compared the liver concentrations of G-6-P and glycogen with liver BBR at each sampling time point. G-6-P reached the maximal concentration 1 h earlier than the  $T_{max}$  of liver BBR (Fig. 4C), and glycogen content increased with the administration of BBR (Fig. 4D). G-6-P is catalyzed by GK, as the distribution of GK is mainly in the liver, and the association of GK and liver BBR levels was also analyzed. The curves of GK activity (Fig. 4E) and mRNA expression (Fig. 4F) showed the same trend as the liver concentration-time curve of BBR and had a positive correlation (correlation factor was 0.473 and 0.873, respectively). Notably, the maximal enzyme activity



Metabolites	Formula	Mol Weight	p-value	q-value	FC
<b>Serum</b>					
Maltose	C <sub>12</sub> H <sub>22</sub> O <sub>11</sub>	342.30	9.22E-03	1.81E-02	-1.12
Ribitol	C <sub>5</sub> H <sub>12</sub> O <sub>5</sub>	152.15	1.73E-02	2.56E-02	-0.98
Xylitol	C <sub>5</sub> H <sub>12</sub> O <sub>5</sub>	152.15	5.78E-03	1.58E-02	-0.61
Ribose	C <sub>5</sub> H <sub>10</sub> O <sub>5</sub>	150.13	1.48E-02	2.37E-02	-0.53
Arabitol	C <sub>5</sub> H <sub>12</sub> O <sub>5</sub>	152.15	7.24E-03	1.70E-02	-0.81
Galactonic acid	C <sub>6</sub> H <sub>12</sub> O <sub>7</sub>	196.16	1.48E-02	2.37E-02	-0.55
Glyceric acid	C <sub>3</sub> H <sub>6</sub> O <sub>4</sub>	106.08	2.81E-02	3.41E-02	-0.37
Pyruvic acid	C <sub>3</sub> H <sub>4</sub> O <sub>3</sub>	88.06	2.19E-02	2.85E-02	-0.49
Glycerol-3-phosphate	C <sub>3</sub> H <sub>5</sub> O <sub>6</sub> P	172.07	3.11E-03	2.85E-02	-0.66
Glycerol-2-phosphate	C <sub>3</sub> H <sub>5</sub> O <sub>6</sub> P	172.07	5.50E-04	3.1E-03	-0.57
Glycerol	C <sub>3</sub> H <sub>8</sub> O <sub>3</sub>	92.09	3.17E-02	3.43E-02	-0.35
<b>Liver</b>					
Glucose	C <sub>6</sub> H <sub>12</sub> O <sub>6</sub>	180.16	1.58E-03	8.4E-03	-0.27
Glucose-6-phosphate	C <sub>6</sub> H <sub>13</sub> O <sub>9</sub> P	260.14	7.45E-03	1.99E-02	0.90
Fructose-6-phosphate	C <sub>6</sub> H <sub>13</sub> O <sub>9</sub> P	260.14	1.59E-02	2.83E-02	-0.37
Gluconic acid	C <sub>6</sub> H <sub>12</sub> O <sub>7</sub>	196.16	3.51E-02	4.45E-02	-0.28
Ribose-5-phosphate	C <sub>5</sub> H <sub>11</sub> O <sub>8</sub> P	230.11	1.49E-02	2.75E-02	-0.4
DHAP	C <sub>3</sub> H <sub>5</sub> O <sub>6</sub> P	168.04	2.85E-03	1.05E-02	-0.95
Glycerate-3-phosphate	C <sub>3</sub> H <sub>6</sub> O <sub>7</sub> P	185.05	2.07E-02	3.31E-02	-0.23
<b>Feces</b>					
Glucose	C <sub>6</sub> H <sub>12</sub> O <sub>6</sub>	180.16	4.33E-03	9.80E-03	-1.55
Gluconic acid	C <sub>6</sub> H <sub>12</sub> O <sub>7</sub>	196.16	4.07E-02	4.18E-02	-2.55
Ribose	C <sub>5</sub> H <sub>10</sub> O <sub>5</sub>	150.13	4.33E-03	9.80E-03	-4.11
Arabitol	C <sub>5</sub> H <sub>12</sub> O <sub>5</sub>	152.15	7.60E-04	6.00E-03	-0.75
Glyceric acid	C <sub>3</sub> H <sub>6</sub> O <sub>4</sub>	106.08	8.66E-03	1.52E-02	-1.51
Pyruvic acid	C <sub>3</sub> H <sub>4</sub> O <sub>3</sub>	88.06	4.33E-03	9.80E-03	-6.96

**Table 1.** Glucose-related metabolites of serum, liver and feces from BBR-treated and untreated *db/db* mice. Note: \*Comparison of differential glucose related metabolites between BBR-treated and untreated *db/db* mice with a Student's *t* test, and all p-values were after FDR correction; FC: fold change was calculated as a binary logarithm of the average mass response (normalized peak area) ratio between BBR-treated and untreated *db/db* mice, where a positive value means that the average mass response of the metabolite in BBR-treated *db/db* mice is larger than that in untreated *db/db* mice.

of GK was 1 h, which was earlier than the  $T_{max}$  of liver BBR. These data suggested that GK activity and expression were sensitive to changes in liver BBR levels.

**BBR upregulated hepatic GK expression in diabetic *db/db* mice.** GK is distributed both in the nucleus and cytoplasm, but only cytoplasmic GK functions, so we detected GK protein in liver lysates, cytoplasm and nucleus. The expression of GK in *db/db* mice was significantly decreased, and BBR treatment restored its expression in all liver portions (Fig. 5A,B). To further observe GK expression, we applied immunohistochemistry staining with GK antibody, and GK-positive areas showed a significant increase in BBR-treated mice compared to the untreated *db/db* mice (Fig. 5C).

GK is encoded by *GCK* (also known as *hexokinase IV*, *HK4*), and we analyzed the mRNA expression of the four *HKs* (*HK1-4*) in the liver. *HK1-4* expression was remarkably decreased in *db/db* mice, and BBR treatment restored *HK4* mRNA expression, which was consistent with the change in GK expression. *HK2* mRNA expression also increased upon BBR treatment (Fig. 5D). In addition, we analyzed gluconeogenesis-related glucose-6-phosphatase (*G6PC*), phosphoenolpyruvate carboxykinase (*PCK1*), AMPK1a (*Prkaal*) and phosphoinositide 3-kinase (*PI3K*), and only *PCK1* expression was suppressed upon BBR treatment (Fig. 5E). We also observed a significant decrease in GLUT2 in *db/db* mice, and BBR partially restored GLUT2 expression (Fig. 5F).

**BBR facilitated GK-GKRP dissociation.** Studies have demonstrated that the activity of GK is regulated by direct binding with GKRP. We also observed increased GKRP in the liver of *db/db* mice; however, the effect of BBR on liver GKRP at the transcriptional and translational levels was negligible (Fig. 6A-D). To further evaluate the binding status of GK and GKRP, we applied a Co-IP experiment, and with identical protein input, we observed that GK expression (Input GK) decreased, GK binding with GKRP (IP GK) increased, and the ratio of IP GK (GK-GKRP binding form)/Input GK increased in *db/db* mice compared with wild-type mice, whereas BBR treatment decreased the ratio, suggesting more GK released from GKRP and could function in glucose metabolism (Fig. 6E,F).

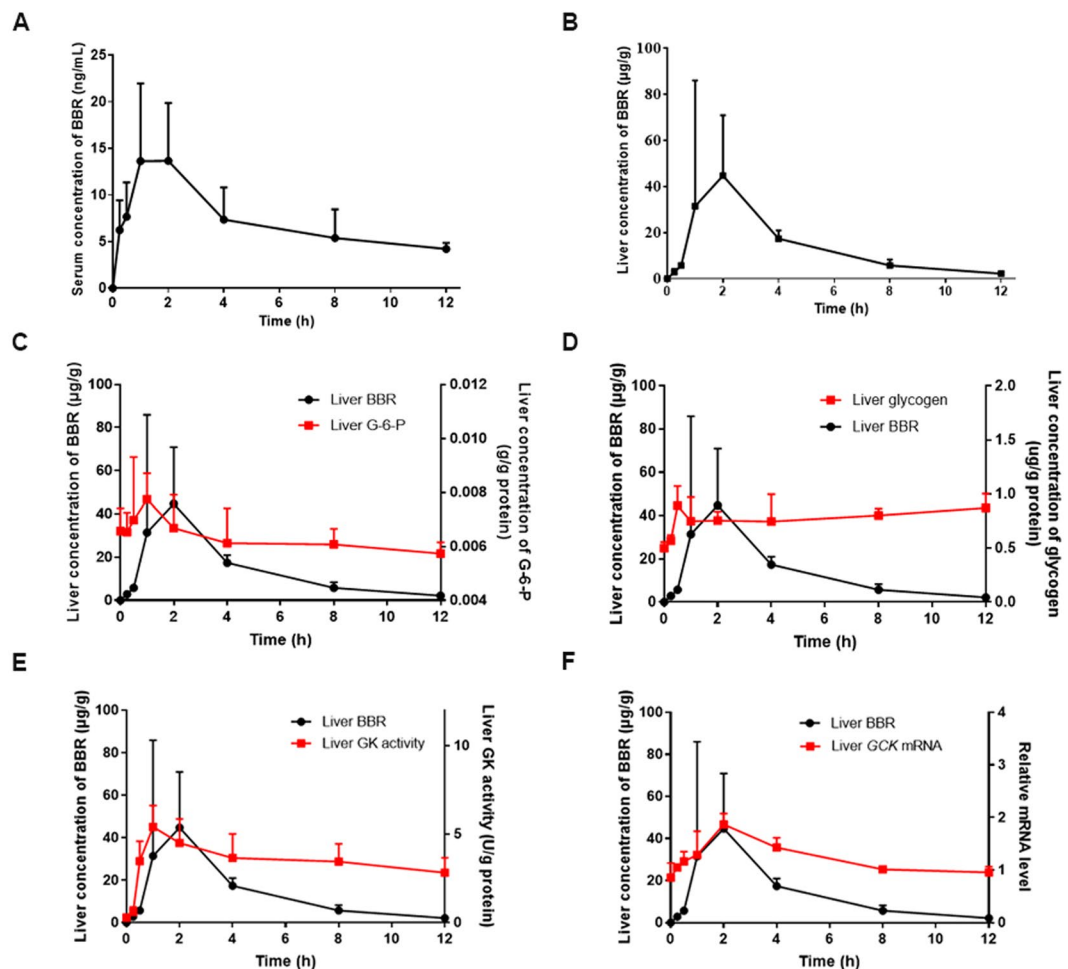


**Figure 4.** PK-PD assessment. Eight-week-old male *db/db* mice were randomly divided into 8 groups ( $n = 5$  per group) and sacrificed at 0.25, 0.5, 1, 2, 4, 8, and 12 h after BBR gavage ( $210 \text{ mg} \cdot \text{kg}^{-1} \cdot \text{day}^{-1}$ ). The untreated mice (0 h) were used as controls. Concentration-time curves of serum (A) and liver (B) BBR are shown. Liver G-6-P (C) and glycogen (D) concentration-time curves, GK activity-time curve (E), and *GCK* expression-time curve (F) were drawn along with the concentration-time curve of liver BBR. The data are presented as the mean  $\pm$  SEM,  $n = 5$  per group.

## Discussion

In the present study, we confirmed that BBR upregulates GK expression in high-glucose cultured AML12 cells and showed the hypoglycemic effect of BBR in *db/db* mice. We obtained increased liver G-6-P/G-1-P through metabolomics detection. PK-PD assessment revealed that both GK activity and expression were positively correlated with liver BBR levels. The increase in liver GK and glycogen content was further verified in BBR-treated *db/db* mice. We also showed increased dissociation of GK from GKRP with BBR treatment. Our results indicated that increased GK release was one of the potential mechanisms of BBR in treating diabetes (Fig. 7).

The glucose-lowering effect of BBR has long been studied. In the 1980s, Chinese researchers accidentally discovered that T2DM patients took BBR as a folk recipe to control their blood glucose, and a small sample investigation further confirmed its effect<sup>16</sup>. From that time, studies of BBR as a T2DM remedy have spread globally. In 2008, a pilot study identified that 3-month BBR treatment could significantly decrease blood glucose and HbA1c in newly diagnosed T2DM patients<sup>17</sup>. Yan *et al.* further confirmed that the anti-diabetic effect of BBR is superior to that of placebo in T2DM patients<sup>18</sup>. The anti-diabetic effects of BBR have also been confirmed in various animal models with T2DM characteristics<sup>19–21</sup>.

Although the therapeutic efficacy of BBR in T2DM was confirmed, the underlying mechanisms of its efficacy are debated due to different study designs, animal strain or race, and patterns of modeling. Diabetic *db/db* mice are the most commonly mice used in T2DM studies. Researchers have also found that adenosine 5'-monophosphate-activated protein kinase (AMPK) in adipocytes and muscle can be activated by BBR, thus promoting peripheral glucose uptake and contributing to its hypoglycemic effect<sup>22</sup>. BBR has also been reported to activate AMPK in macrophages and other peripheral tissues to alleviate metabolic-related stress in *db/db* mice<sup>23,24</sup>. By orally administering BBR to *db/db* mice, Li *et al.* found that BBR improved diabetic characteristics by increasing SIRT1 protein expression and alleviating endoplasmic reticulum stress<sup>25</sup>. In high-fat diet fed ICR

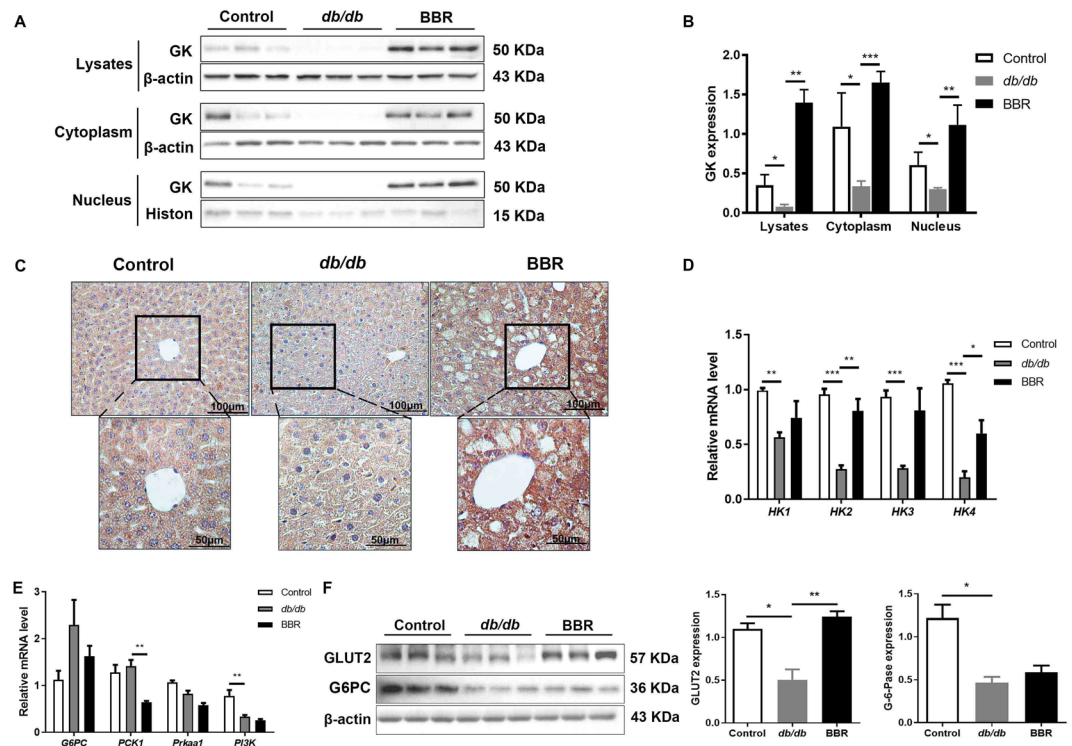


**Figure 5.** BBR upregulated hepatic GK expression in *db/db* mice. Western blot analysis (A) and qualification (B) of GK in liver lysates, cytoplasm and nucleus. (C) Immunohistochemistry staining for GK in liver sections. The mRNA levels of *HK1-4*, *G6PC*, *PCK1*, *Prkaa1* and *PI3K* were quantified by qRT-PCR (D,E). (F) Hepatic GLUT2 and G-6-Pase were detected by Western blot. The groupings were cropped from different gels subjected to identical conditions. Data are presented as the mean  $\pm$  SEM,  $n = 3$  per group. \* $P < 0.05$ , \*\* $P < 0.01$ , and \*\*\* $P < 0.001$  between groups.

mice, BBR is reported to inhibit SIRT3 to reduce hepatic glucose production<sup>26</sup>. Hepatic gluconeogenesis is also supported by BBR in diabetic status, and key gluconeogenesis enzymes, such as PCK and G6PC, can be reduced by BBR, indicating the inhibition of gluconeogenesis upon BBR intervention<sup>14,27</sup>.

Metabolomics have been developed and widely applied in biological studies since the 1990s. In studying the mechanisms of BBR in diabetes, metabolites of samples from both T2DM patients and animals have been analyzed, and certain fatty acids were identified to be involved<sup>18,28</sup>. Here we noticed the alteration in G-6-P/G-1-P and identified GK as the target by retrieval and verification. Hepatic GK expression is physiologically regulated by fasting and refeeding cycles and is pathologically reduced in diabetes<sup>29,30</sup>. The levels of insulin, glucagon and glucocorticoids all affect the activity of GK, while GK activation works dramatically on glucose metabolic pathways<sup>31-33</sup>. The accumulated G-6-P/G-1-P due to GK activation could be further transformed into glycogen or utilized for energy. Corresponding to the upregulation of G-6-P/G-1-P, we also observed increased hepatic glycogen content upon BBR treatment in *db/db* mice, which restored insufficient glycogen reserve in diabetic status, consistent with previous studies<sup>15,34</sup>. Excessive glycogen in the liver is correlated with numerous diseases, such as glycogen storage disease type I (GSD I), also known as Von Gierke disease, for which deficiency of specific enzymes is the main cause<sup>35</sup>. Although some gastrointestinal symptoms occurred in BBR clinical trials<sup>36,37</sup>, no reports of BBR-related liver glycogen excess were found.

Previous studies showed that GKRPs posttranscriptionally regulate GK function in hepatocytes via binding and dissociating processes<sup>38,39</sup>. The GKRPs seemed unaffected by BBR at both the transcriptional and translational levels. Such an inconsistency might be due to the animals or feeding, and the sample processing methods may also be related. Another study also reported that the deacetylation of GKRPs contributes to the facilitation of hepatic glucose uptake<sup>8,38,40</sup>. Our data suggest that GK is the dominant target of BBR in regulating hepatic glucose uptake.

In conclusion, we confirmed an increase in liver GK and hypoglycemia upon BBR treatment. GK activity and expression were positively related to liver BBR levels, and GK increase was associated with GK release from GKRPs, which contributed to the anti-diabetic effect of BBR.

## Methods

**Materials.** BBR hydrochloride (purity  $\geq 99\%$ ) was purchased from Shanghai Ronghe Pharmaceutical Technology Development Company (Shanghai, China). L-leucine-<sup>13</sup>C<sub>6</sub>-<sup>15</sup>N, L-isoleucine-<sup>13</sup>C<sub>6</sub>-<sup>15</sup>N, L-valine-<sup>13</sup>C<sub>5</sub>-<sup>15</sup>N, L-alanine-<sup>13</sup>C<sub>3</sub>-<sup>15</sup>N, methoxylamine hydrochloride, dulcitol and N,O-bis(trimethylsilyl)-trifluoroacetamide (BSTFA) with 1% trimethylchlorosilane (TMCS) were purchased from Sigma-Aldrich (St. Louis, MO, USA). Methanol, ethanol and isopropanol for HPLC grade were purchased from Merck Chemicals (Darmstadt,

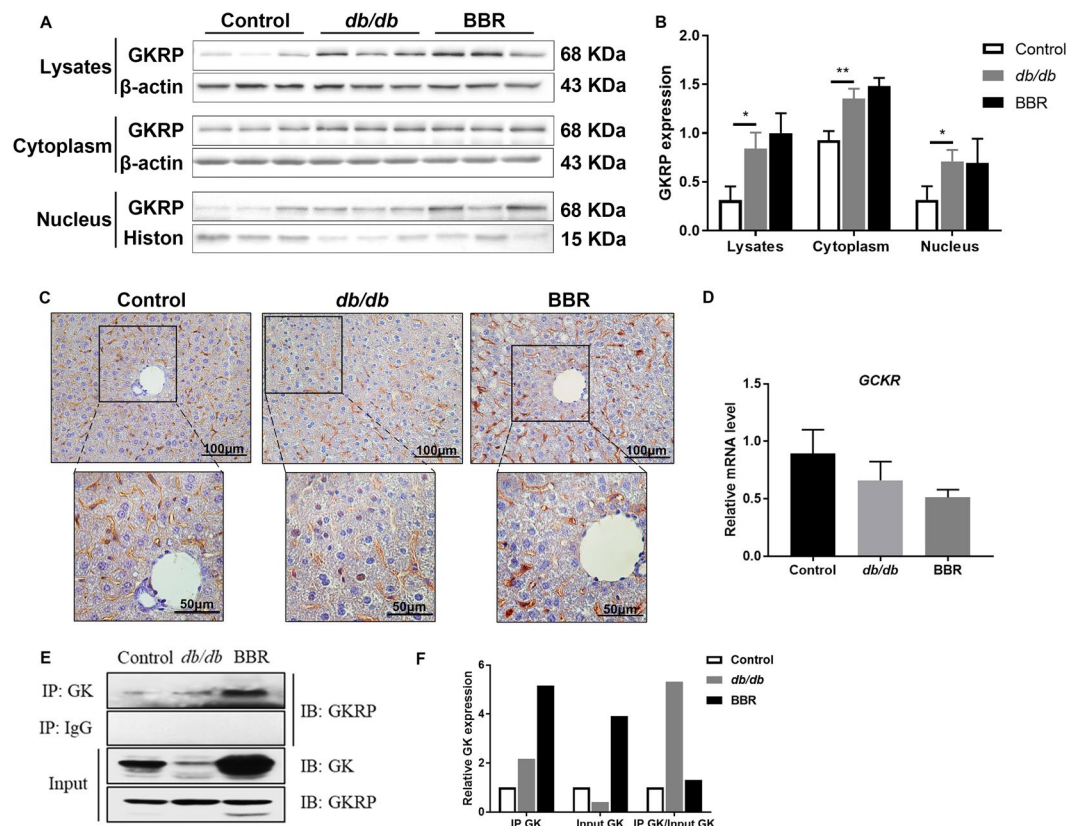


**Figure 6.** BBR increased GK-GKRP dissociation. Western blot analysis (A) and qualification (B) of GKRP in liver lysates, cytoplasm and nucleus. (C) Immunohistochemistry staining for GKRP in liver sections. (D) The mRNA level of *GCKR* was quantified by qRT-PCR. Liver lysates were immunoprecipitated (E) and quantified (F) by an anti-GK antibody, and immunoblotting was performed to detect the binding status of GK and GKRP. The groupings were cropped from different gels subjected to identical conditions. Data are presented as the mean  $\pm$  SEM,  $n = 3$  per group. \* $P < 0.05$  and \*\* $P < 0.01$  between groups.

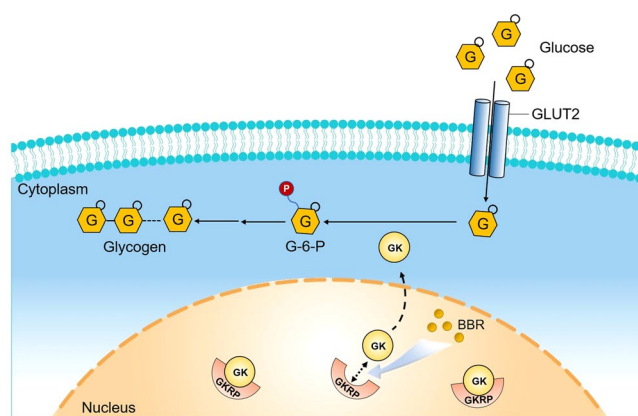


**Figure 7.** Potential mechanisms of GK increase due to the anti-diabetic property of BBR. Through increasing GK release from GKRP, BBR upregulated hepatic GK expression and increased glucose uptake and glycogen content in the liver, thus exerting an anti-diabetic effect in *db/db* mice.



Germany). Chloroform of analytical grade was purchased from Sinopharm Chemical Reagent Company (Shanghai, China). Trizol reagent was purchased from Invitrogen (Carlsbad, CA, USA).

**Animals.** Eight-week-old male C57BL/6J wild-type (20–25 g,  $n = 10$ ) and leptin receptor-mutated (C57BL/KsJ-*db/db*) mice (35–40 g,  $n = 18$ ) were purchased from the Model Animal Research Center of Nanjing University (Nanjing, China). Animals were acclimatized in specific pathogen-free rooms at a temperature of 20–26 °C, humidity of 30–70% and a 12-h light/dark cycle for one week. All animal experiments were performed in accordance with the approved guidelines of the Experimental Animal Care and Ethics of Animal Experiments Committee of Shanghai University of Traditional Chinese Medicine (Shanghai, China).

After one week of acclimatization, *db/db* mice were randomly divided into two groups based on blood glucose: the untreated group (*db/db* group,  $n = 8$ ) and the BBR treatment group (BBR group,  $n = 10$ ). BBR (210 mg·kg<sup>-1</sup>·day<sup>-1</sup>) was suspended in 0.5% sodium carboxy methylcellulose (CMC-Na) solution and then administered to the treated mice, while the untreated mice were given an equal volume of 5% CMC-Na solution for 4 weeks. Regular laboratory chow and filtered tap water were allowed ad libitum, and the mice fasted 12 h before sacrifice.

**Biochemical analysis of serum and liver tissue.** After four weeks of treatment, the mice were anesthetized with 2% sodium pentobarbital, blood was obtained and the serum was separated by centrifugation for 15 min at 3000 rpm. Levels of insulin, glucagon and HbA1c were measured using mouse ELISA kits (Shanghai Enzyme-linked Biotechnology Company, Shanghai, China). Blood glucose was measured by an automated biochemical analyzer.

The liver was rapidly removed, weighed, and washed with precooled normal saline, and a fraction of the same position was cut and fixed in 10% formalin, while remaining fractions were stored at -80 °C after being snap-frozen in liquid nitrogen. Liver glycogen was analyzed using an assay kit (Dongou Technologies Company, Zhejiang, China) according to the manufacturer's instructions and read with UV-mini1240 spectrophotometer (Shimadzu, Kyoto, Japan).

**Liver histological and immunohistochemical analysis.** Liver fractions were fixed in formalin overnight and embedded in paraffin wax. Paraffin sections (4 μm) were prepared for PAS (Solarbio, Beijing, China) staining to observe the pathological changes and glycogen storage. For immunohistochemical analysis, liver sections were pretreated with citrate buffer, incubated with anti-GK (Santa Cruz Biotechnology, sc-17819) and anti-GKRP (Santa Cruz Biotechnology, sc-166841) antibodies overnight at 4 °C, and then polymerized horseradish peroxidase-conjugated secondary antibodies were added to visualize the positive area. Images were captured using a system incorporated in a Nikon Eclipse 50i microscope with magnification of 200x, and representative areas were further shown with magnification of 400x.

**Metabolomic profile.** The process of sample preparation, gas chromatography-mass spectrometry (GC-MS) analysis, data processing, bioinformatics and statistical analysis were conducted as previously described<sup>41</sup>. In brief, the serum, liver and feces were prepared, added with internal standards, dried under a gentle nitrogen stream, incubated with methoxylamine hydrochloride in anhydrous pyridine, derivatized with BSTFA (with 1% TMCS) and then splitlessly injected into an Agilent 7890 A series GC coupled to an HP-5MS column (30 m × 0.25 mm, 0.25 film thickness) and an Agilent 5975 C inert MSD detector. The GC-MS data were processed with DataBridge (Perkin-Elmer, USA), and multivariate statistical analysis was applied with SIMCA-P 11.0 software (Umetrics AB, Umeå, Sweden) to perform PCA and PLS-DA. The differential metabolites and metabolic pathways were determined using the Golm Metabolome and KEGG Database.

**Immunoblotting.** Liver tissues were homogenized in ice-cold radioimmune precipitation (RIPA) lysis buffer (Beyotime Institute of Biotechnology, Shanghai, China) with protease and phosphatase inhibitors. Nuclear and cytoplasmic fractions were obtained using the nuclear and cytoplasmic protein extraction kit (Beyotime). Protein lysates were separated on 10% SDS-PAGE, transferred to polyvinylidene difluoride (PVDF) membranes (Millipore, Temecula, CA), and immunoblotted with the following primary antibodies: GK (sc-17819, 1:1000), GKRP (sc-166841, 1:1000) and G-6-Pase (sc-15840, 1:1000), which were purchased from Santa Cruz Biotechnology (CA, USA), and an antibody against GLUT2 (ab544460, 1:1000), which was purchased from Abcam (Cambridge, MA, USA). As a loading control, β-actin (4970, 1:1000) was purchased from Cell Signaling Technology (Beverly, MA, USA) and histone (ab8580, 1:1000) was purchased from Abcam. For secondary antibodies: anti-mouse IgG (14709, 1:3000) and anti-rabbit IgG (5127, 1:3000) were obtained from Cell Signaling Technology. Blot bands were quantified using the Chemi Fluorescent and Chemiluminescent Imaging System (Syngene, Cambridge, UK). The groupings of the blots cropped from different gels subjected to identical conditions, and the full-length gels are shown in Supplementary Fig. S1.

**Co-Immunoprecipitation (Co-IP).** Liver tissue was lysed with RIPA buffer, centrifuged, and precleared with protein A/G agarose beads (Santa Cruz). Supernatants were collected and immunoprecipitated overnight with anti-GK antibody (sc-17819, Santa Cruz) or negative control IgG antibody (Boster Biol Tech, Wuhan, China). After overnight incubation, protein A/G agarose beads were added, pelleted by centrifugation, washed three times with ice-cold washing buffer, boiled for 5 min, and subjected to electrophoresis, and GKRP expression was analyzed by immunoblotting. The groupings of the blots cropped from different gels subjected to identical conditions, and the full-length gels are shown in Supplementary Fig. S1.

**Quantitative RT-PCR.** Total RNA was extracted from liver tissue using Trizol reagent. cDNA was reverse-transcribed with the high capacity reverse transcription kit from Applied Biosystems (Monza, Italy) and

used in RT-PCR with SYBR Green PCR Master Mix (Toyobo, Japan) in a StepOne Applied PCR system. The data were analyzed by the  $2^{-\Delta\Delta Ct}$  method, and samples were normalized to glyceraldehyde-3-phosphate dehydrogenase (GAPDH). The primer sequences are listed in Supplementary Table S2.

**Cell culture and glycogen storage detection.** Mouse AML12 hepatocytes were obtained from the Cell Bank of the Chinese Academy of Sciences (Shanghai, China), and cultured in Dulbecco's modified Eagle's medium (DMEM)/F12 (GIBCO, 11330-032) supplemented with 10% (v/v) fetal bovine serum (FBS), 1% (v/v) ITS liquid media supplement (sigma, I3146) and 40 ng/ml dexamethasone (Sigma, D4902). The cells were incubated at 37 °C in an incubator continuously supplying 5% CO<sub>2</sub>.

After incubation of mouse AML12 hepatocytes without or with 20 μM BBR for 24 h at 37 °C, we determined glycogen content with hepatocyte ELISA kits (Shanghai Enzyme-linked Biotechnology Company). Protein content was measured as well, and glycogen content was expressed as mg/g protein. Cells were fixed with 4% formaldehyde and a PAS staining kit (Solarbio) was used to evaluate glycogen storage.

**Immunofluorescence.** AML12 hepatocytes were treated with or without BBR (1, 5, or 20 μM). The cells were then fixed with 4% paraformaldehyde (w/v), permeabilized with 0.5% Triton X-100, and incubated with blocking buffer containing 10% bovine serum albumin (BSA) for 2 h at room temperature. Next, the cells were incubated overnight at 4 °C with GK antibody containing 10% BSA, washed with phosphate buffer saline (PBS), and incubated in the dark for 2 h with Alexa Fluor 488-conjugated goat anti-mouse secondary antibodies (Invitrogen). After washing with PBS, the nucleus was stained with 2-(4-amidinophenyl)-6-indolecarbamidine dihydrochloride (DAPI) for 10 min, and images were taken by an Olympus IX71 fluorescence microscope.

**PK-PD study of BBR in *db/db* mice.** Eight-week-old male C57BL/KsJ-*db/db* mice were randomly divided into 8 groups (n = 5 per group) and sacrificed at 0.25, 0.5, 1, 2, 4, 8, and 12 h after BBR gavage (210 mg·kg<sup>-1</sup>·day<sup>-1</sup>). The untreated mice (0 h) were used as controls. All animals were fasted 12 h before administration of BBR. At each time point, animals were anesthetized, and blood and liver tissues were collected.

10% liver tissue homogenate of *db/db* mice was prepared by adding 10 mL saline to 1 g liver tissue. A 50-μL aliquot of serum/homogenate and 200 μL acetonitrile containing 50 ng/mL IS was vortexed for 2 min and then centrifuged at 12,000 × g for 5 min. Then, 10 μL of the aliquot was injected into the liquid chromatography-tandem mass spectrometry (LC-MS/MS) system to analyze the concentration of BBR, and the method was performed as previously described<sup>42</sup>.

All calibration and quantitation data were processed with MassHunter Workstation Qualitative Analysis Software Version B.04.00. The serum/tissue concentration-time data were analyzed using noncompartmental methods with the software program PK solutions 2™ (Summit Research Services, USA) to determine pharmacokinetic parameters. A Pearson correlation analysis was performed using SPSS 18.0. Liver glycogen was analyzed, and G-6-P and GK activity were analyzed using an ELISA kit (Westang Biotechnology company, Shanghai, China). GCK expression was measured.

**Statistical analysis.** Quantitative data are expressed as the mean ± SEM. Statistically significant differences were assessed using two-tailed Student's *t*-test or one-way ANOVA. SPSS 18.0 statistical software (SPSS, Chicago, IL, USA) was used for statistical analysis. Values of *P* < 0.05 were considered statistically significant.

## Data Availability

All data generated or analyzed during this study are included in this published article (and its Supplementary Information file).

## References

- Unnikrishnan, R., Pradeepa, R., Joshi, S. R. & Mohan, V. Type 2 Diabetes: Demystifying the Global Epidemic. *Diabetes* **66**, 1432–1442, <https://doi.org/10.2337/db16-0766> (2017).
- Ogurtsova, K. *et al.* IDF Diabetes Atlas: Global estimates for the prevalence of diabetes for 2015 and 2040. *Diabetes Res Clin Pract* **128**, 40–50, <https://doi.org/10.1016/j.diabres.2017.03.024> (2017).
- Leclercq, I. A., Morais, D. S., Schroyen, A., Van Hul, B. & Geerts, N. A. Insulin resistance in hepatocytes and sinusoidal liver cells: mechanisms and consequences. *J Hepatol* **47**, 142–156, <https://doi.org/10.1016/j.jhep.2007.04.002> (2007).
- Postic, C., Dentin, R. & Girard, J. Role of the liver in the control of carbohydrate and lipid homeostasis. *Diabetes Metab* **30**, 398–408 (2004).
- Rizza, R. A. Pathogenesis of fasting and postprandial hyperglycemia in type 2 diabetes: implications for therapy. *Diabetes* **59**, 2697–2707, <https://doi.org/10.2337/db10-1032> (2010).
- Moore, M. C., Coate, K. C., Winnick, J. J., An, Z. & Cherrington, A. D. Regulation of hepatic glucose uptake and storage *in vivo*. *Adv Nutr* **3**, 286–294, <https://doi.org/10.3945/an.112.002089> (2012).
- Zheng, Y., Ley, S. H. & Hu, F. B. Global aetiology and epidemiology of type 2 diabetes mellitus and its complications. *Nat Rev Endocrinol* **14**, 88–98, <https://doi.org/10.1038/nrendo.2017.151> (2018).
- Rubtsov, P. M., Igudin, E. L. & Tiulpakov, A. N. [Glucokinase and glucokinase regulatory proteins as molecular targets for novel antidiabetic drugs]. *Molekuliarnaia biologii* **49**, 555–560, <https://doi.org/10.7868/S002689841504014X> (2015).
- Hale, C., Lloyd, D. J., Pellacani, A. & Veniant, M. M. Molecular targeting of the GK-GKRP pathway in diabetes. *Expert Opin Ther Targets* **19**, 129–139, <https://doi.org/10.1517/14728222.2014.965681> (2015).
- Tjokropawiro, A. New approach in the treatment of T2DM and metabolic syndrome (focus on a novel insulin sensitizer). *Acta Med Indones* **38**, 160–166 (2006).
- Scheen, A. J. Investigational insulin secretagogues for type 2 diabetes. *Expert Opin Investig Drugs* **25**, 405–422, <https://doi.org/10.1517/13543784.2016.1152260> (2016).
- Peng, Y., Chen, S. H., Liu, X. N. & Sun, Q. Y. Efficacy of different antidiabetic drugs based on metformin in the treatment of type 2 diabetes mellitus: A network meta-analysis involving eight eligible randomized-controlled trials. *J Cell Physiol*, <https://doi.org/10.1002/jcp.27097> (2018).

13. Zhang, H. *et al.* Berberine lowers blood glucose in type 2 diabetes mellitus patients through increasing insulin receptor expression. *Metabolism* **59**, 285–292, <https://doi.org/10.1016/j.metabol.2009.07.029> (2010).
14. Xia, X. *et al.* Berberine improves glucose metabolism in diabetic rats by inhibition of hepatic gluconeogenesis. *PLoS One* **6**, e16556, <https://doi.org/10.1371/journal.pone.0016556> (2011).
15. Xie, X. *et al.* Berberine ameliorates hyperglycemia in alloxan-induced diabetic C57BL/6 mice through activation of Akt signaling pathway. *Endocrine journal* **58**, 761–768 (2011).
16. Ni, Y. X. [Therapeutic effect of berberine on 60 patients with type II diabetes mellitus and experimental research]. *Zhong Xi Yi Jie He Za Zhi* **8**(711–713), 707 (1988).
17. Yin, J., Xing, H. & Ye, J. Efficacy of berberine in patients with type 2 diabetes mellitus. *Metabolism* **57**, 712–717, <https://doi.org/10.1016/j.metabol.2008.01.013> (2008).
18. Gu, Y. *et al.* Effect of traditional Chinese medicine berberine on type 2 diabetes based on comprehensive metabolomics. *Talanta* **81**, 766–772, <https://doi.org/10.1016/j.talanta.2010.01.015> (2010).
19. Jia, Y., Xu, B. & Xu, J. Effects of type 2 diabetes mellitus on the pharmacokinetics of berberine in rats. *Pharm Biol* **55**, 510–515, <https://doi.org/10.1080/13880209.2016.1255649> (2017).
20. Zhang, Y. *et al.* Treatment of type 2 diabetes and dyslipidemia with the natural plant alkaloid berberine. *J Clin Endocrinol Metab* **93**, 2559–2565, <https://doi.org/10.1210/jc.2007-2404> (2008).
21. Chandrasegaran, G., Elanchezhiyan, C. & Ghosh, K. Effects of Berberine chloride on the liver of streptozotocin-induced diabetes in albino Wistar rats. *Biomed Pharmacother* **99**, 227–236, <https://doi.org/10.1016/j.biopha.2018.01.007> (2018).
22. Lee, Y. S. *et al.* Berberine, a natural plant product, activates AMP-activated protein kinase with beneficial metabolic effects in diabetic and insulin-resistant states. *Diabetes* **55**, 2256–2264, <https://doi.org/10.2337/db06-0006> (2006).
23. Kim, W. S. *et al.* Berberine improves lipid dysregulation in obesity by controlling central and peripheral AMPK activity. *Am J Physiol Endocrinol Metab* **296**, E812–819, <https://doi.org/10.1152/ajpendo.90710.2008> (2009).
24. Jeong, H. W. *et al.* Berberine suppresses proinflammatory responses through AMPK activation in macrophages. *Am J Physiol Endocrinol Metab* **296**, E955–964, <https://doi.org/10.1152/ajpendo.90599.2008> (2009).
25. Li, H. Y. *et al.* Berberine Improves Diabetic Encephalopathy Through the SIRT1/ER Stress Pathway in db/db Mice. *Rejuvenation Res* **21**, 200–209, <https://doi.org/10.1089/rej.2017.1972> (2018).
26. Li, A. *et al.* Berberine Reduces Pyruvate-driven Hepatic Glucose Production by Limiting Mitochondrial Import of Pyruvate through Mitochondrial Pyruvate Carrier 1. *EBioMedicine* **34**, 243–255, <https://doi.org/10.1016/j.ebiom.2018.07.039> (2018).
27. Wei, S. *et al.* Berberine Attenuates Development of the Hepatic Gluconeogenesis and Lipid Metabolism Disorder in Type 2 Diabetic Mice and in Palmitate-Incubated HepG2 Cells through Suppression of the HNF-4alpha miR122 Pathway. *PLoS One* **11**, e0152097, <https://doi.org/10.1371/journal.pone.0152097> (2016).
28. Dong, Y. *et al.* Metabolomics Study of Type 2 Diabetes Mellitus and the AntiDiabetic Effect of Berberine in Zucker Diabetic Fatty Rats Using Uplc-ESI-Hdms. *Phytother Res* **30**, 823–828, <https://doi.org/10.1002/ptr.5587> (2016).
29. Iynedjian, P. B., Gjinovci, A. & Renold, A. E. Stimulation by insulin of glucokinase gene transcription in liver of diabetic rats. *J Biol Chem* **263**, 740–744 (1988).
30. Magnuson, M. A., Andreone, T. L., Printz, R. L., Koch, S. & Granner, D. K. Rat glucokinase gene: structure and regulation by insulin. *Proc Natl Acad Sci USA* **86**, 4838–4842 (1989).
31. Wang, Z. S. *et al.* [Effect of berberine on insulin secretion and glucokinase activity of NIT-1 cells]. *Yao xue xue bao = Acta pharmaceutica Sinica* **42**, 1045–1049 (2007).
32. Zhang, X. *et al.* Dose selection using a semi-mechanistic integrated glucose-insulin-glucagon model: designing phase 2 trials for a novel oral glucokinase activator. *Journal of pharmacokinetics and pharmacodynamics* **40**, 53–65, <https://doi.org/10.1007/s10928-012-9286-9> (2013).
33. Egea, M., Meton, I., Cordoba, M., Fernandez, F. & Baanante, I. V. Role of Sp1 and SREBP-1a in the insulin-mediated regulation of glucokinase transcription in the liver of gilthead sea bream (*Sparus aurata*). *General and comparative endocrinology* **155**, 359–367, <https://doi.org/10.1016/j.ygcen.2007.06.018> (2008).
34. Zhou, J. Y. *et al.* Chronic effects of berberine on blood, liver glucolipid metabolism and liver PPARs expression in diabetic hyperlipidemic rats. *Biological & pharmaceutical bulletin* **31**, 1169–1176 (2008).
35. Parikh, N. S. & Ahlawat, R. In *StatPearls* (2018).
36. Cicero, A. F. *et al.* Berberine and monacolin effects on the cardiovascular risk profile of women with oestrogen-induced hypercholesterolemia. *High Blood Press Cardiovasc Prev* **21**, 221–226, <https://doi.org/10.1007/s40292-014-0052-5> (2014).
37. Lan, J. *et al.* Meta-analysis of the effect and safety of berberine in the treatment of type 2 diabetes mellitus, hyperlipemia and hypertension. *Journal of ethnopharmacology* **161**, 69–81, <https://doi.org/10.1016/j.jep.2014.09.049> (2015).
38. Kaminski, M. T. *et al.* Glucose-induced dissociation of glucokinase from its regulatory protein in the nucleus of hepatocytes prior to nuclear export. *Biochimica et biophysica acta* **1843**, 554–564, <https://doi.org/10.1016/j.bbamcr.2013.12.002> (2014).
39. Ashton, K. S. *et al.* Small molecule disruptors of the glucokinase-glucokinase regulatory protein interaction: 1. Discovery of a novel tool compound for *in vivo* proof-of-concept. *Journal of medicinal chemistry* **57**, 309–324, <https://doi.org/10.1021/jm4016735> (2014).
40. Watanabe, H. *et al.* Sirt2 facilitates hepatic glucose uptake by deacetylating glucokinase regulatory protein. *Nature communications* **9**, 30, <https://doi.org/10.1038/s41467-017-02537-6> (2018).
41. Li, M. *et al.* Integrative analysis of metabolome and gut microbiota in diet-induced hyperlipidemic rats treated with berberine compounds. *J Transl Med* **14**, 237, <https://doi.org/10.1186/s12967-016-0987-5> (2016).
42. Zhang, Q., Ma, Y. M., Wang, Z. T. & Wang, C. H. Pharmacokinetics difference of multiple active constituents from decoction and maceration of Fuzi Xiexin Tang after oral administration in rat by UPLC-MS/MS. *J Pharm Biomed Anal* **92**, 35–46, <https://doi.org/10.1016/j.jpba.2013.12.038> (2014).

## Acknowledgements

We have appreciated Professor C.H. Wang and Y.L. Lu for the help in PK/PD experiment. This study was supported by the National Nature Science Foundation of China (No. 81620108030, 81774084, and 81803897).

## Author Contributions

G.J. and L.Z. designed the study. M.L., Q.L., W.J.Z. performed the animal experiment and collected related data. M.L. and Y.Q.D. performed the *in vitro* experiment. Z.M.Y. and J.P.Z. helped the data interpretation. L.Z. and M.L. interpreted the data, drafted and edited the manuscript. G.J. supervised the whole process. All authors approved the final version of the paper.

## Additional Information

**Supplementary information** accompanies this paper at <https://doi.org/10.1038/s41598-019-44576-7>.

**Competing Interests:** The authors declare no competing interests.

**Publisher's note:** Springer Nature remains neutral with regard to jurisdictional claims in published maps and institutional affiliations.



**Open Access** This article is licensed under a Creative Commons Attribution 4.0 International License, which permits use, sharing, adaptation, distribution and reproduction in any medium or format, as long as you give appropriate credit to the original author(s) and the source, provide a link to the Creative Commons license, and indicate if changes were made. The images or other third party material in this article are included in the article's Creative Commons license, unless indicated otherwise in a credit line to the material. If material is not included in the article's Creative Commons license and your intended use is not permitted by statutory regulation or exceeds the permitted use, you will need to obtain permission directly from the copyright holder. To view a copy of this license, visit <http://creativecommons.org/licenses/by/4.0/>.

© The Author(s) 2019